Supporting Information for

Impacts of Cascading Check Dams on Sediment Yield in the Middle Yellow River Basin: Insights from 50 Years of Grid-cell-level Simulation

Yanzhang Huang[1,2], Guangyao Gao[1,2,4,5,*], Lishan Ran[3], Yue Wang[1,2], Mingguo Zheng[6]

[1]State Key Laboratory of Regional and Urban Ecology, Research Center for Eco-Environmental Sciences, Chinese Academy of Sciences, Beijing 100085, China

[2]University of Chinese Academy of Sciences, Beijing 100049, China

[3]Department of Geography, The University of Hong Kong, Hong Kong 999077, China

[4]National Observation and Research Station of Earth Critical Zone on the Loess Plateau in Shaanxi, Xi'an, China

[5]Shaanxi Yan'an Forest Ecosystem Observation and Research Station, Beijing 100085, China

[6]Guangdong Key Laboratory of Integrated Agro-environmental Pollution Control and Management, Institute of Eco-environmental and Soil Sciences, Guangdong Academy of Sciences, Guangzhou 510650, China

Contents of this file

Introduction

The texts include the methodological description for implementing the soil erosion estimation (Text S1) and the methodological description for the trade-off analysis (Text S2). The figures include the parameter calibration results of IC0 and Kic for each sub-basin (Figure S1), the temporal and spatial results of soil erosion (Figures S2 and S3), the results of the intermediate parameters IC and SDR used to calculate sediment yield (Figures S4 and S5), the spatial distribution and temporal changes in the sediment trapping efficiency of check dams (Figure S6), detailed sediment-yield maps after accounting for sediment interception (Figure S7), and the temporal dynamics of sediment reduction contribution and sediment deposition across sub-basins (Figures S8 and S9). The tables provide basic information for the 17 hydrological stations and the empirical assignment scheme for the P factor (Tables S1 and S2).

Text S1. Calculation of each factor in RUSLE

To improve the accuracy of erosion calculations, we first calculated the erosion rate on a monthly scale using the RUSLE model, and then summed these up to obtain the annual erosion rate:

$$E = R \cdot K \cdot LS \cdot C \cdot P \quad (1)$$

where E is the soil erosion (t ha^{-1} yr^{-1}), R is the rainfall erosivity (MJ mm ha^{-1} h^{-1} yr^{-1}) factor, K is the soil erodibility (Mg ha h MJ^{-1} ha^{-1} mm^{-1}) factor, L is the slope length factor, S is the slope steepness factor, C is the land cover and management factor, and P is the soil conservation or prevention practice factor.

The R factor was calculated using the method of Xie et al., (2016) with the daily rainfall data of CHM_PRE. The erosivity of daily rainfall was calculated according to j month. The model is a power-law equation based on the sinusoidal relation reflecting the seasonal variation of coefficient α:

$$R_{day} = 0.2686\left[1 + 0.5412\,cos\left(\frac{\pi}{6}j - \frac{7\pi}{6}\right)\right]P_d^{1.7265} \quad (2)$$

where R_{day} (MJ mm ha^{-1} h^{-1} yr^{-1}) is daily rainfall erosivity; j presents the jth month; P_d (mm) is the daily effective rainfall (≥ 9.7 mm).

The K factor was calculated according to the recommendations of the EPIC model (EPIC: The erosion-productivity impact calculator).

$$K = 0.1317 \cdot (0.2 + 0.3 \cdot e^{[-0.0256 \cdot San \cdot (1 - \frac{Sil}{100})]}) \cdot (\frac{Sil}{Cla + Sil})^{0.3} \cdot [1 - \frac{0.25 \cdot TOC}{TOC + e^{(3.72 - 2.95 \cdot TOC)}}] \cdot [1 - \frac{0.7 \cdot SN_1}{SN_1 + e^{(22.9 \cdot SN_1 - 5.51)}}] \quad (3)$$

where K (t ha h MJ^{-1} mm^{-1} ha^{-1}) is the soil erodibility; *San* (%) is the sand content (0.05–2 mm); *Sil* (%) is the silt content (0.002–0.05 mm); *Cla* (%) is the clay content (< 0.002 mm); *TOC* (%) is the soil total organic carbon content; and SN_1 = 1–*San*/100. After multiplying by 0.1317, the K value is expressed in an SI metric (t ha h MJ^{-1} mm^{-1} ha^{-1}). For soil samples with organic matter content (TOC=SOM×0.58) above 4%, the upper limit of 4% has been applied, to prohibit an underestimation of soil erodibility for soils that are rich in organic matter (Panagos et al., 2015; Wischmeier and Smith, 1978).

The *LS* factor was calculated using the method developed by Böhner & Selige (2006) in SAGA-Analyses and modelling applications. Firstly, DEM should be filled sinks in ArcGIS using Fill tool. Then Flow Accumulation tool is used to calculate total Catchment Area (TCA) in ASGA, and Flow Width and Specific Catchment Area tool is used to calculate Specific Catchment Area (SCA). Finally, SAGA's LS factor was used to calculate the LS factor (Schürz et al., 2020).

The advantage of using NDVI is to determine the monthly dynamics of factor *C*. Thereby we could understand the impact of vegetation cover on seasonal soil erosion and identify the critical periods of the year for soil erosion risk (Benavidez et al., 2018). Especially in large-scale research, due to the lack of sufficient field investigation, the calculation of *C* factor by NDVI has a good application prospect. The most widely used method to calculate the *C* factor according to NDVI is the exponential form equation proposed by van der Knijff et al. (2000) with α = -2 and β = 1.

$$C = exp\left[\alpha\left(\frac{NDVI}{\beta - NDVI}\right)\right] \quad (4)$$

The *P* factor was assigned empirical values based on land use types, terraced distribution, and slope data (Table S2).

Text S2. Trade-off analysis method between sediment reduction contribution and sediment accumulation amount of check dams

Bradford and D'Amato (2012) have elucidated a straightforward approach for quantifying the consequences of different management scenarios based on the trade-offs and benefits among multiple objectives. This method has been widely employed in balancing two or more management objectives (Chen et al., 2022; Langner et al., 2017; Su et al., 2021). We initially standardized the sediment reduction contribution of check dams (SRC_{dam}) and the proportion of accumulated sediment relative to total reservoir capacity (i.e., sediment accumulation ratio, SAR_{dam}) to eliminate the dimensional relationship between variables. The standardized environmental variables, also regarded as the relative benefits of environmental variables, are defined as (Bradford and D'Amato, 2012):

$$X_{std} = (X_{obs} - X_{min})/(X_{max} - X_{min}) \quad (5)$$

where X_{std} is the standardized value of a management objective, X_{obs} is the observation value of the management objective, X_{min} and X_{max} are the minimum and maximum value of the management objective. Overall benefit is calculated as the mean of individual benefits and increases from low benefit in the lower left to greater benefit in the upper right (Bradford and D'Amato, 2012). Trade-off is calculated as the root mean squared error of the individual benefits and increases with distance from the 1:1 line.

References

Benavidez, R., Jackson, B., Maxwell, D., and Norton, K.: A review of the (Revised) Universal Soil Loss Equation ((R)USLE): With a view to increasing its global applicability and

improving soil loss estimates, Hydrol. Earth Syst. Sci., 22, 6059–6086, https://doi.org/10.5194/hess-22-6059-2018, 2018.

Böhner, J. and Selige, T.: Spatial prediction of soil attributes using terrain analysis and climate regionalisation, Göttinger Geogr. Abhandlungen, 115, 13–28, 2006.

Bradford, J. B. and D'Amato, A. W.: Recognizing trade-offs in multi-objective land management, Front. Ecol. Environ., 10, 210–216, https://doi.org/10.1890/110031, 2012.

Chen, Y., Wei, T., Ren, K., Sha, G., Guo, X., Fu, Y., and Yu, H.: The coupling interaction of soil organic carbon stock and water storage after vegetation restoration on the Loess Plateau, China, J. Environ. Manage., 306, 114481, https://doi.org/10.1016/j.jenvman.2022.114481, 2022.

van der Knijff, J. M., Jones, R. J. A., and Montanarella, L.: Soil erosion risk assessment in Europe, 2000.

Langner, A., Irauschek, F., Perez, S., Pardos, M., Zlatanov, T., Öhman, K., Nordström, E. M., and Lexer, M. J.: Value-based ecosystem service trade-offs in multi-objective management in European mountain forests, Ecosyst. Serv., 26, 245–257, https://doi.org/10.1016/j.ecoser.2017.03.001, 2017.

Panagos, P., Borrelli, P., Poesen, J., Ballabio, C., Lugato, E., Meusburger, K., Montanarella, L., and Alewell, C.: The new assessment of soil loss by water erosion in Europe, Environ. Sci. Policy, 54, 438–447, https://doi.org/10.1016/j.envsci.2015.08.012, 2015.

Schürz, C., Mehdi, B., Kiesel, J., Schulz, K., and Herrnegger, M.: A systematic assessment of uncertainties in large-scale soil loss estimation from different representations of USLE input factors-a case study for Kenya and Uganda, Hydrol. Earth Syst. Sci., 24, 4463–4489, https://doi.org/10.5194/hess-24-4463-2020, 2020.

EPIC: The erosion-productivity impact calculator: http://agris.fao.org/agris-search/search.do?recordID=US9403696.

Su, B., Su, Z., and Shangguan, Z.: Trade-off analyses of plant biomass and soil moisture relations on the Loess Plateau, Catena, 197, 104946, https://doi.org/10.1016/j.catena.2020.104946, 2021.

Wischmeier, W. H. and Smith, D. D.: Predicting rainfall erosion losses: A guide to conservation planning (Agriculture Handbook No. 537), 1978.

Xie, Y., Yin, S., Liu, B., Nearing, M. A., and Zhao, Y.: Models for estimating daily rainfall erosivity in China, J. Hydrol., 535, 547–558, https://doi.org/10.1016/j.jhydrol.2016.02.020, 2016.

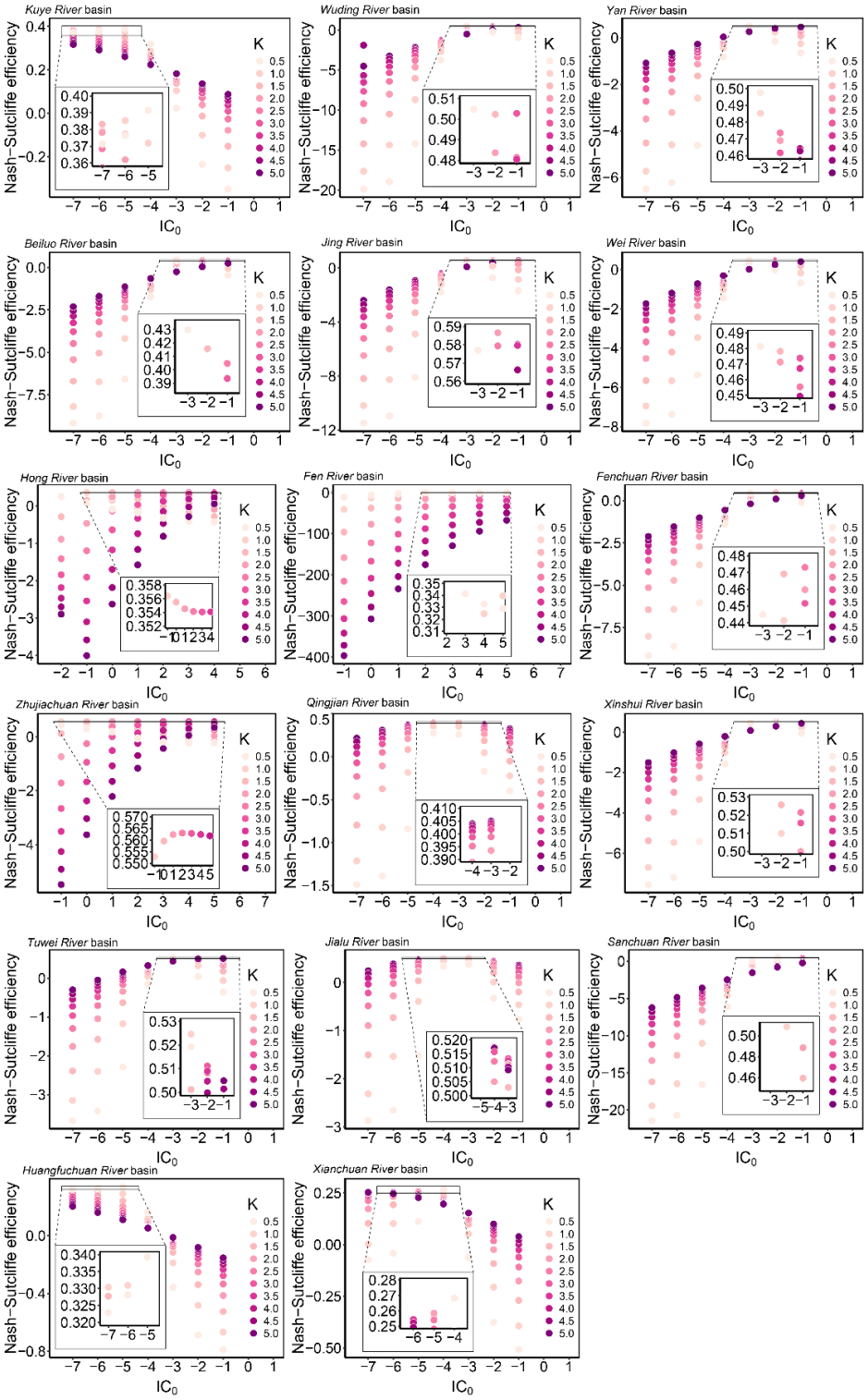

Figure S1. Calibration of IC_0 and K_{IC} parameter combinations for 17 sub-basins in the middle Yellow River Basin. The detailed inset reveals the optimal parameter combinations.

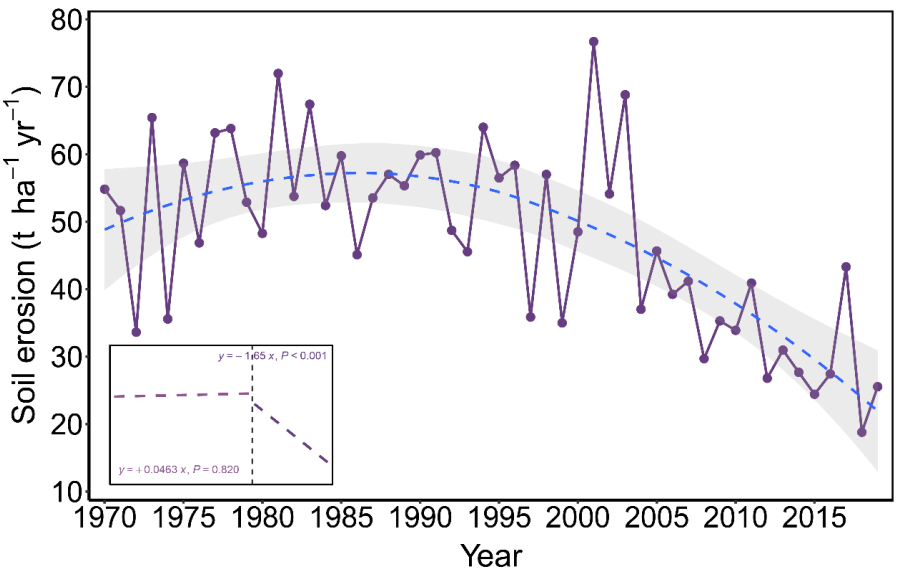

Figure S2. Interannual variations in average soil erosion rate of the middle Yellow River Basin from 1970 to 2020. The inset in the lower left displays the linear regression of soil erosion rate before and after 2001. The dashed line represents a fitted curve with the shaded area indicating the 95% confidence interval.

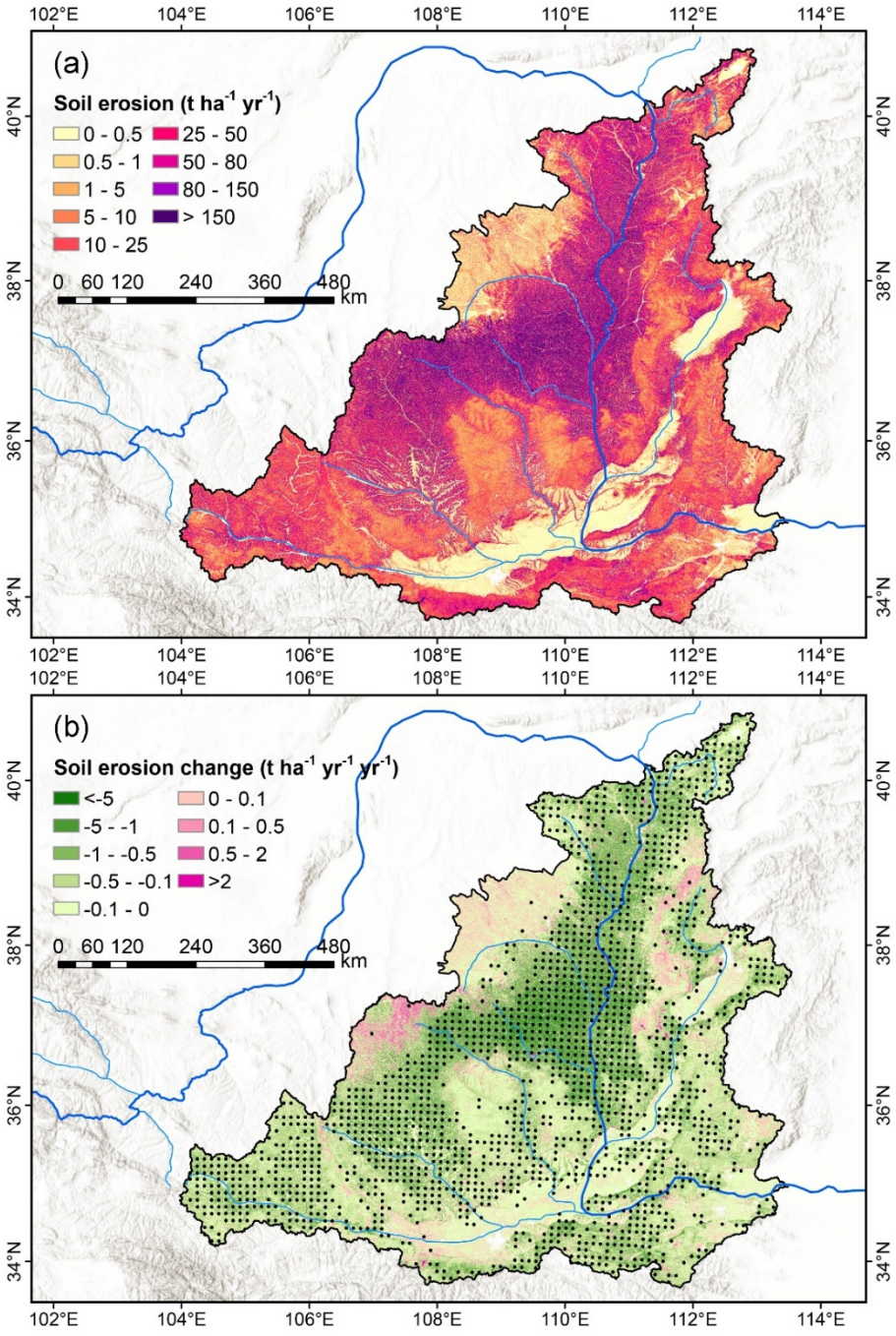

Figure S3. Spatial distribution of (a) average soil erosion during 1970-2020 and (b) soil erosion change over the 50-year period in the middle Yellow River Basin. Black dots in (b) mark areas with significant changes in soil erosion ($P < 0.05$).

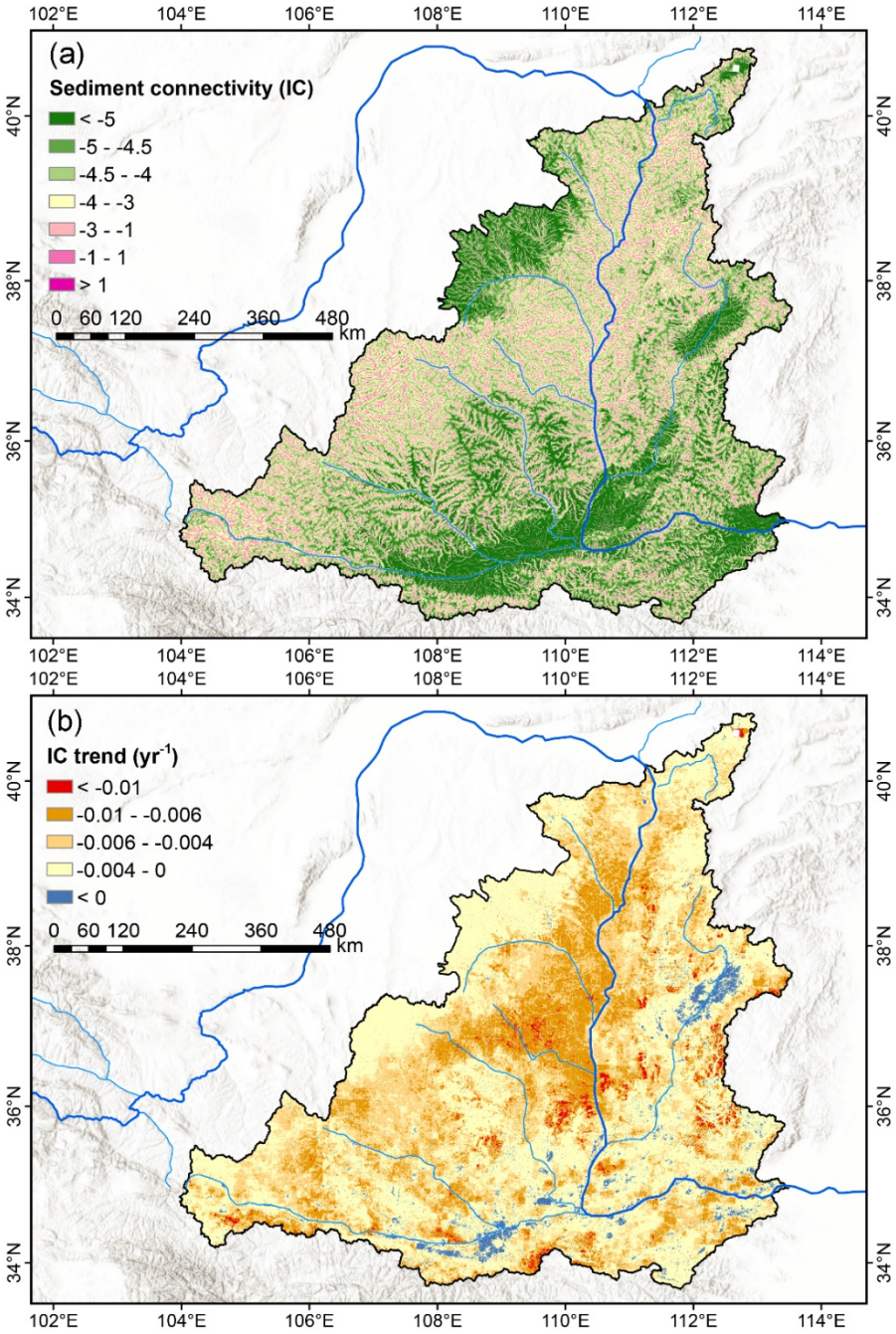

Figure S4. Spatial distribution of (a) average sediment connectivity (IC) during 1970-2020 and (b) trends of IC over the 50-year period in the middle Yellow River Basin.

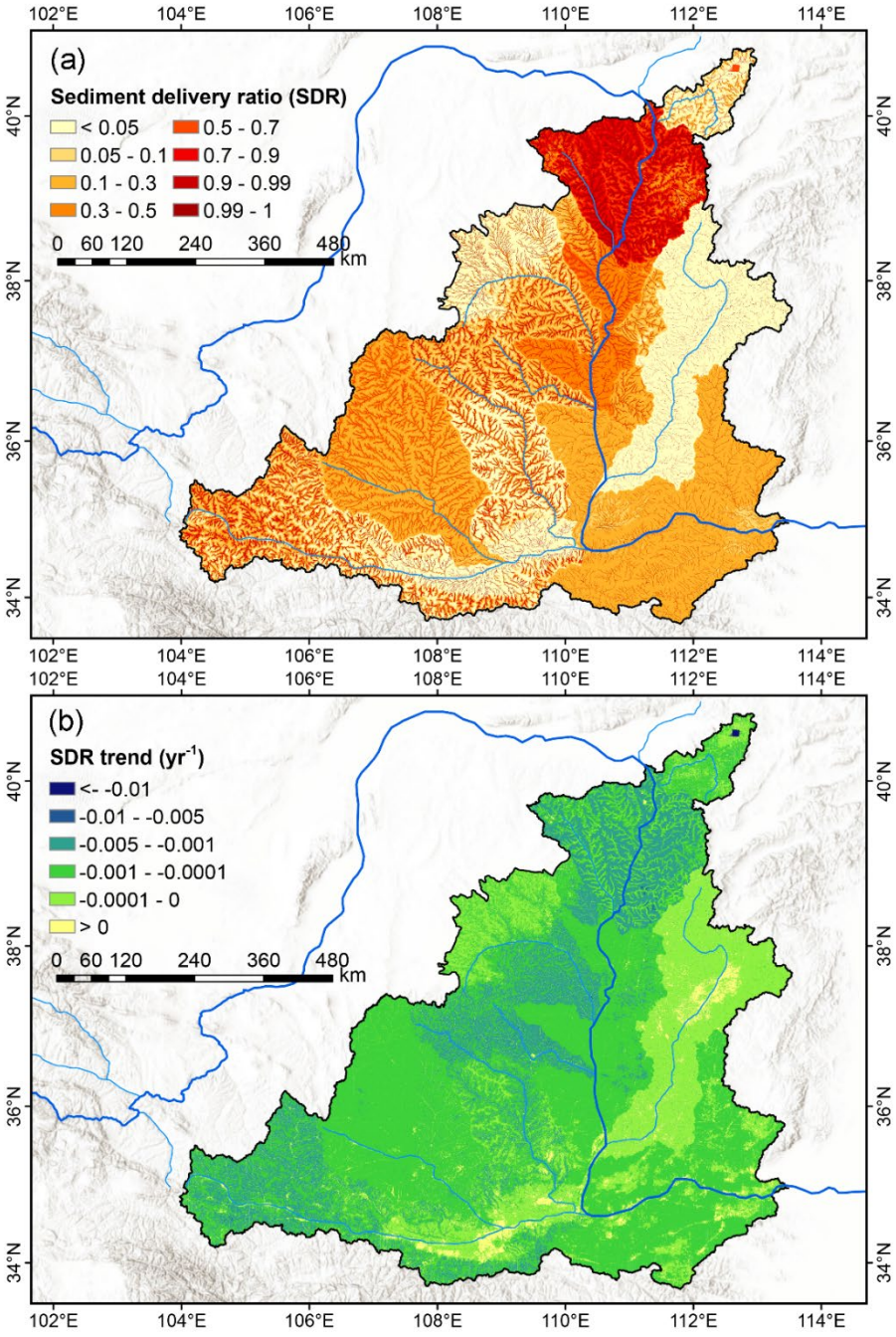

Figure S5. Spatial distribution of (a) average sediment delivery ratio (SDR) during 1970-2020 (b) and trends of SDR over the 50-year period in the middle Yellow River Basin.

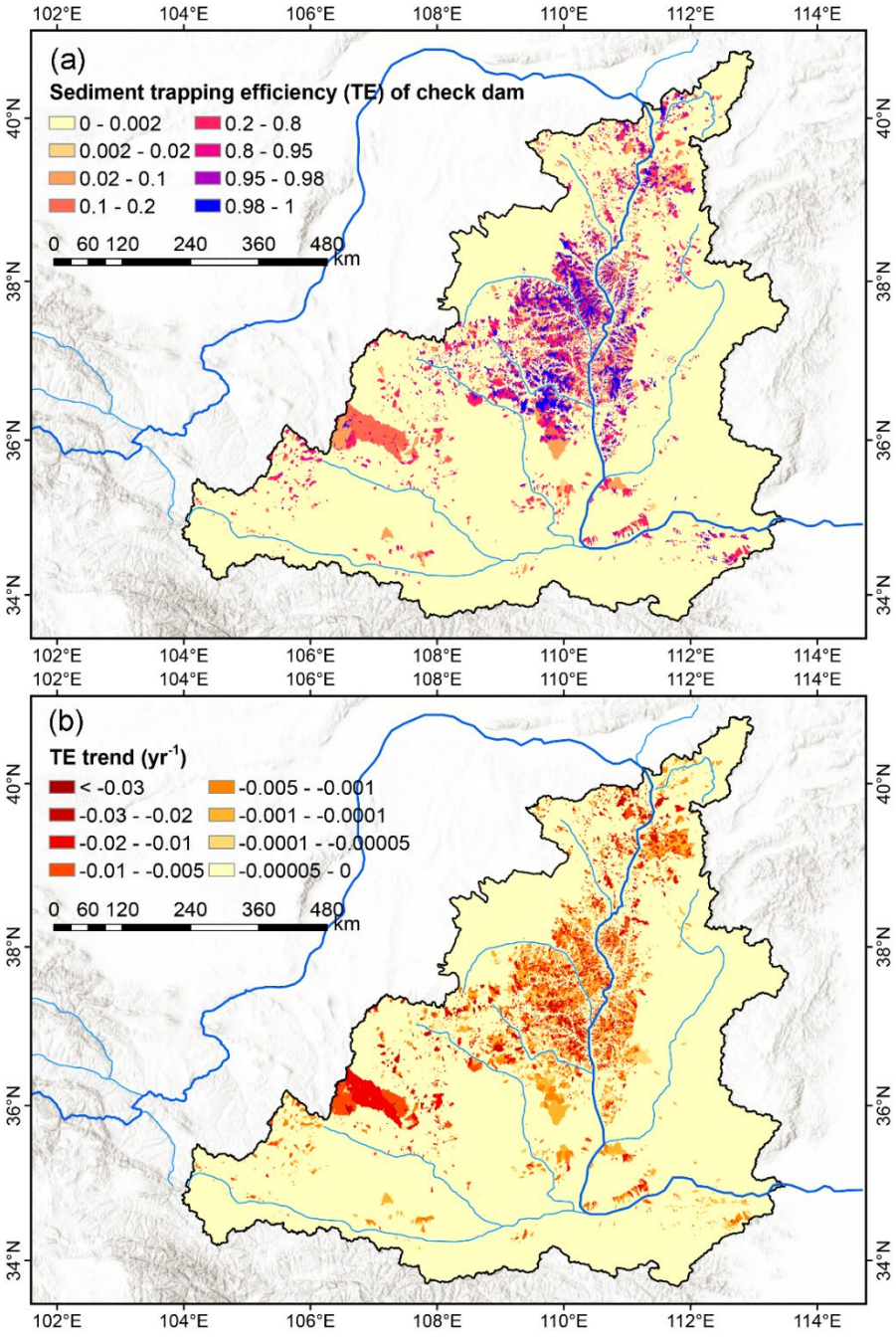

Figure S6. Spatial distribution of (a) average sediment trapping efficiency (TE) of check dams during 1970-2020 and (b) trends of TE over the 50-year period in the middle Yellow River Basin.

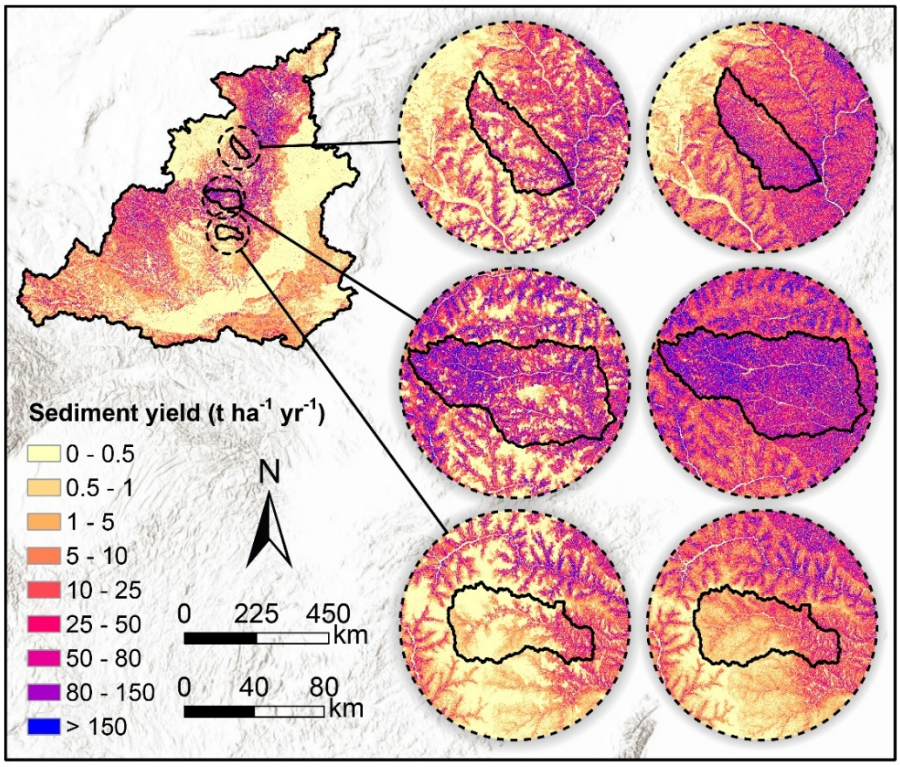

Figure S7. Detailed illustration of the multi-year average sediment yield (SY) incorporating the sediment trapping of check dams in the middle Yellow River Basin. The circular inset on the left provides an enlarged view of the spatial distribution of SY for three selected sub-basins. For comparison, the SY without sediment trapping for the same sub-basin is shown on the right. The upper and lower scale bars represent the main map scale and the enlarged view scale, respectively.

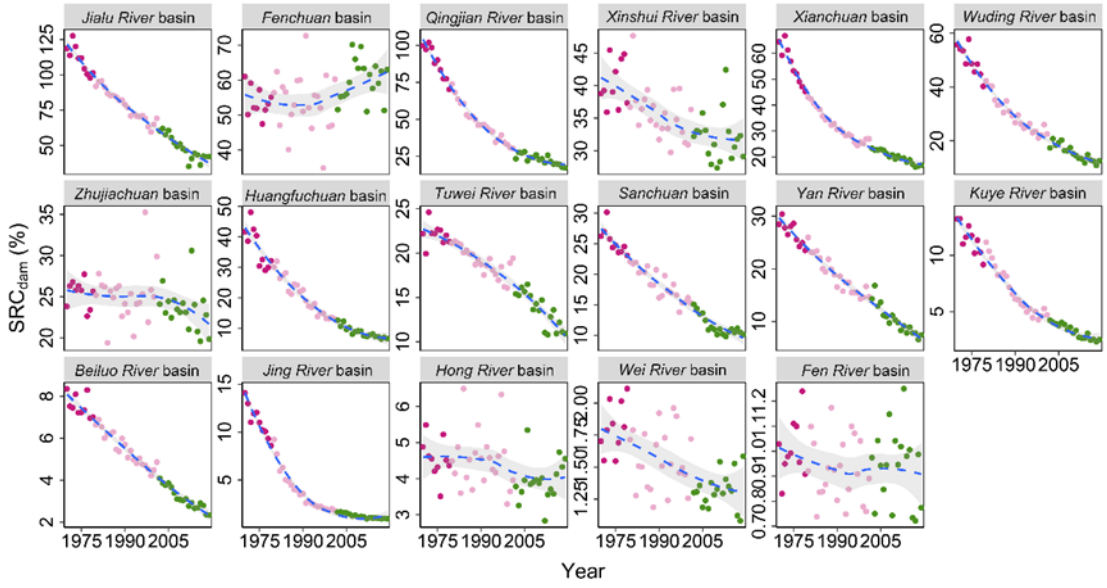

Figure S8. Interannual variation in the sediment reduction contribution by check dams (SRC_{dam}) for the 17 sub-basins in in the middle Yellow River Basin. The three different colors represent sediment yield during 1970-1979, 1980-2001, and 2002-2020.

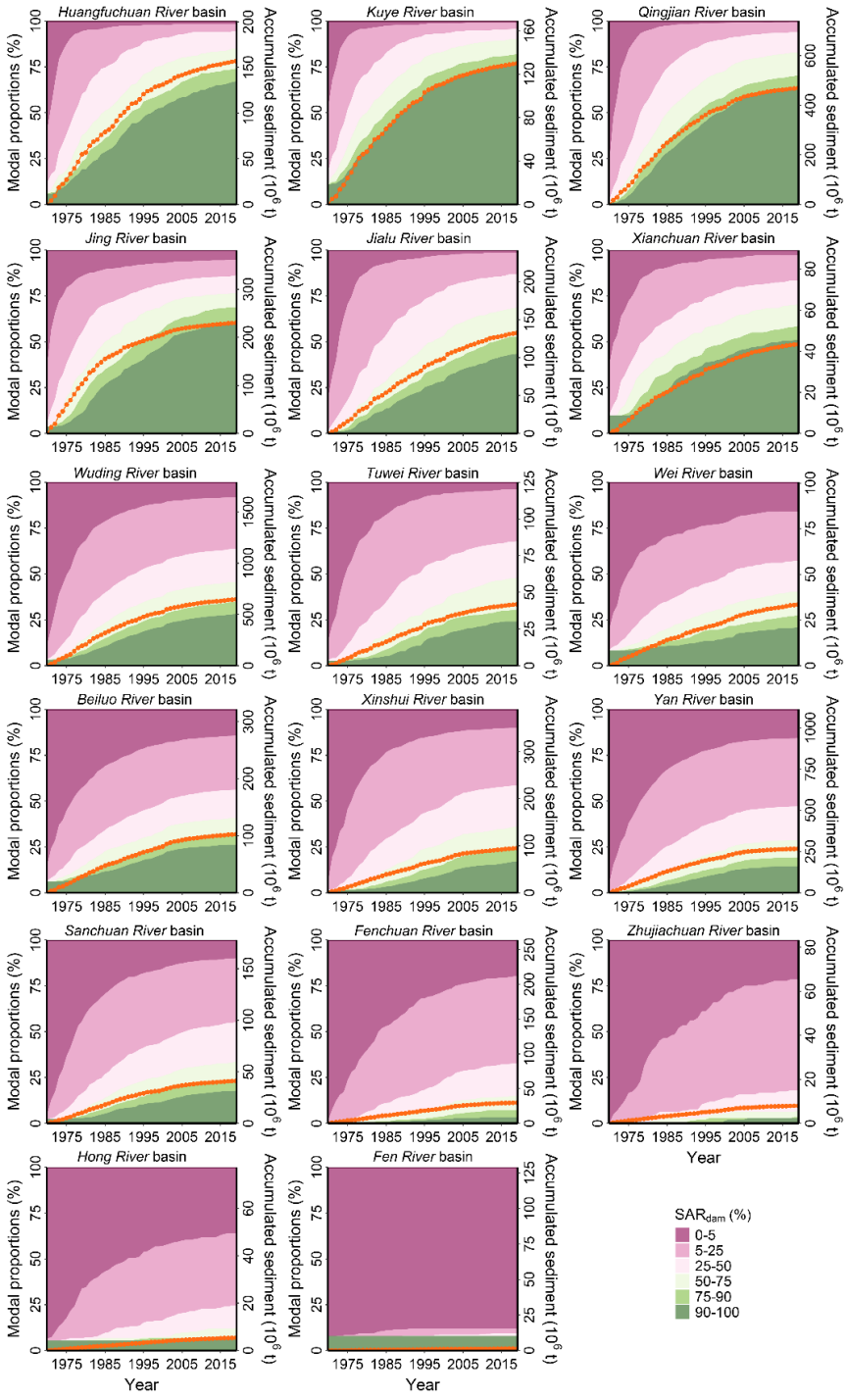

Figure S9. Modal proportions of check dams characterized by different proportions of accumulated sediment relative to total storage capacity (SAR_{dam}) (colored fill), alongside annual changes in accumulated sediment in check dams (orange dotted line) across the 17 sub-basins in the middle Yellow River Basin.

Table S1. Overview of 17 sub-basins controlled by hydrological stations in the middle Yellow River Basin.

No.	Sub-basin	Hydrological station	Area (km^2)	Observed sediment yield ($t\ ha^{-1}\ yr^{-1}$)	Number of check dams
1	Huangfuchuan River	Huangfuchuan	3174.46	55.74	462
2	Kuye River	Wenjiachuan	8651.64	35.99	959
3	Tuwei River	Gaojiachuan	4989.40	14.93	628
4	Jialu River	Shenjiawan	1119.08	35.50	1042
5	Wuding River	Baijiachuan	29622.99	16.25	9471
6	Qingjian River	Yanchuan	3126.31	56.35	2409
7	Yan River	Ganguyi	5817.08	35.91	2157
8	Fenchuan River	Xinshihe	1660.14	10.82	705
9	Zhujiachuan River	Dacun	2139.75	3.04	144
10	Beiluo River	Zhuangtou	25666.54	17.23	1395
11	Jing River	Zhangjiashan	43203.11	26.41	745
12	Wei River	Xianyang	46803.14	8.42	374
13	Hong River	Dangyangqiao	7047.13	5.00	267
14	Xianchuan River	Jiuxian	1562.13	22.51	561
15	Sanchuan River	Houdacheng	4103.75	12.93	918
16	Xinshui River	Daning	3986.84	11.67	1582
17	Fen River	Hejin	38880.22	0.53	441

Table S2. The *P* factor in the RUSLE model based on land use type, slope and terraced distribution.

Land use	Slope/terraces	*P* value
Cropland	0–6°/terraces	0.2
	6–15°	0.35
	15–25°	0.65
	>25°	0.8
Forest and grassland	terraces	0.2
	-	1
Waterbody	-	1
Built land	-	0
Other	-	1